

Topological Patterns

David Apigo¹, Camelia Prodan¹ and Emil Prodan²

¹*Department of Physics, New Jersey Institute of Technology, Newark, NJ 07102, USA*

²*Department of Physics, Yeshiva University, New York, NY 10016, USA*

Abstract

The research in topological materials and meta-materials reached maturity and is now gradually entering the phase of practical applications and devices. However, scaling down the experimental demonstrations definitely presents a challenge. In this work, we study coupled identical resonators whose collective dynamics is fully determined by the pattern in which the resonators are arranged. We call a pattern topological if boundary resonant modes fully fill all existing spectral gaps whenever the pattern is halved. This is a characteristic of the pattern and is entirely independent of the structure of the resonators and the details of the couplings. Existence of such patterns is proven using K -theory and exemplified using a novel experimental platform based on magnetically coupled spinners. Topological meta-materials built on these principles can be easily engineered at any scale, providing a practical platform for applications and devices.

I. INTRODUCTION

Experimental demonstrations of topological effects in classical mechanical system abound [1–24]. The field is definitely ripe to enter the next stage where practical devices and concrete applications are ought to emerge. There is, however, a major impediment because the topological vibrational effects are collective phenomena, hence they occur in extended systems. To be practical, the building blocks of a topological meta-material then need to be scaled down to microns in order to fit a device of a few centimeters square. Maintaining control over the design, however, becomes increasingly difficult and many existing experimental platforms effectively have no chance of achieving this practical scale.

In this work we demonstrate that topological properties can emerge solely from a smart patterning of the meta-materials. Without any tuning of the couplings besides the opening of gaps in the bulk resonant vibrational spectrum, we will show that, for certain patterns, all the bulk spectral gaps of a meta-material become completely filled with topological edge spectrum when the system is halved. This edge spectrum cannot be gapped by any boundary condition or by adiabatic deformation of the meta-material. For this reason, we call them topological patterns. Due to such minimal requirements, meta-materials designed on these principles may be indeed fabricated at any scale, hence providing a viable pathway towards concrete practical applications.

The main goal of our exposition is two fold. On one hand, we want to demonstrate the experimental manifestation of one such topological pattern and, on the other hand, we want to explain the theoretical principles behind these unusual predictions. Regarding the first aspect, we introduce a novel experimental platform based on magnetically coupled spinners. Its hallmark feature resides in the fact that we can build arbitrarily complex mechanical resonators and couplings by adding one degree of freedom at a time. This will be amply discussed in Section II. The experimental platform will not only enable us to realize and characterize a topological pattern of mechanical resonators but also to formulate and exemplify the theoretical concepts which otherwise could appear quite abstract.

The topological patterns are necessarily aperiodic and, as such, the traditional Bloch-

Floquet analysis cannot be used. The natural theoretical tool to use in these situations is the K -theory of C^* -algebras. In this work, we build on the fundamental works of Jean Bellissard [25] and of Kellendonk, Richter and Schulz-Baldes [26] and formulate a K -theoretic bulk-boundary principle for generically patterned resonators. This principle enables us to resolve the precise conditions in which topological edge spectrum emerges as well as the mechanism behind this phenomenon. Prediction of topological patterns then becomes a routine. For simplicity, the present study is restricted to one-dimensional patterns but generalizations to higher dimensions can be easily achieved based on [27]. These will be reported in separate publications.

Our exposition is organized as follows. In Section II we introduce the experimental platform based on magnetically coupled spinners. In particular, we show how to quantitatively map the coupling functions and to ultimately obtain the dynamical matrices that drive the dynamics of the collective resonant modes when the spinners are assembled in arbitrary patterns. We use this concrete setting to explain what topological classification over a fixed pattern means and give the first hints to why such program is feasible, despite the fact that the pattern can be arbitrary. In particular, we show that all dynamical matrices take a very specific form involving only a limited set of operators. This leads us to introduce in Section III the bulk algebra which generates all possible dynamical matrices via a canonical representation. For the proposed patterns, we compute this algebra explicitly and show that it is isomorphic to the algebra generated by magnetic translations. In Section IV we illustrate the bulk spectra of the proposed patterns and point to the similarity with the Hofstadter butterfly [28]. We also illustrate the good agreement between numerical and experimental mappings of the spectra. To rationalize the complexity of the spectra, we review Bellissard's gap labeling procedure [29] and show how to compute bulk topological invariants solely from the integrated density of states. It is at this point where the K -theory is introduced. Section V is dedicated to the edge analysis. In the first part, we illustrate the manifestation of the topological edge spectrum through both numerical simulations and experimental observation. The second part is devoted to explaining the K -theoretic bulk-boundary mechanism, which culminates with the proof that indeed the proposed patterns are topological. A discussion of possible applications concludes the exposition.

Lastly, let us map the relation between our and other existing works. To our knowledge, the emergence of topological boundary spectrum in quasi-periodic structures was first point out theoretically and observed experimentally in [30, 31]. Questions about these systems were raised in [32], namely, the issue was if the topological characteristics noted in [30] are a property of one pattern or of an ensemble of patterns? Answers were provided in [33] using some of the algebraic methods employed in the present work. By passing from numerical topological invariants to the K -theory groups, here we will answer those questions completely and, furthermore, a complete picture of all possible topological systems over a quasi-periodic pattern will emerge. Additionally, we provide the first experimental observation of such topological edge modes in a quasi-periodic mechanical system. Let us point out that our work is part of the vigorous effort of the meta-materials community on the search for topological boundary resonances in aperiodic systems [30–50]. This exploration goes well beyond the periodic table of topological insulators and superconductors [51–53].

II. MAGNETICALLY COUPLED SPINNERS: A VERSATILE EXPERIMENTAL PLATFORM

Here we introduce a novel experimental platform which can be easily reconfigured and quantitatively characterized in a laboratory. It enables us to engineer patterns of coupled mechanical resonators with predefined internal structures and couplings, and to study the spectral properties of virtually any imaginable discrete model. The experimental control over these system is extremely high, resulting in an excellent agreement between theory and experiment. One particular configuration will be discussed in detail to exemplify the experimental procedures. This configuration will be subsequently used to demonstrate a topological pattern. The experimental platform will also be used to introduce the program of topological classification over an aperiodic pattern and other more abstract concepts.

A. Coupling and dynamics

A configurable spinner is illustrated in Fig. 1(a). It consists of a stainless steel ball-bearing mounted in a brass encapsulation. The latter is fitted with grooved indentations that enable us to decorate the spinners with a multitude of components. The centers of

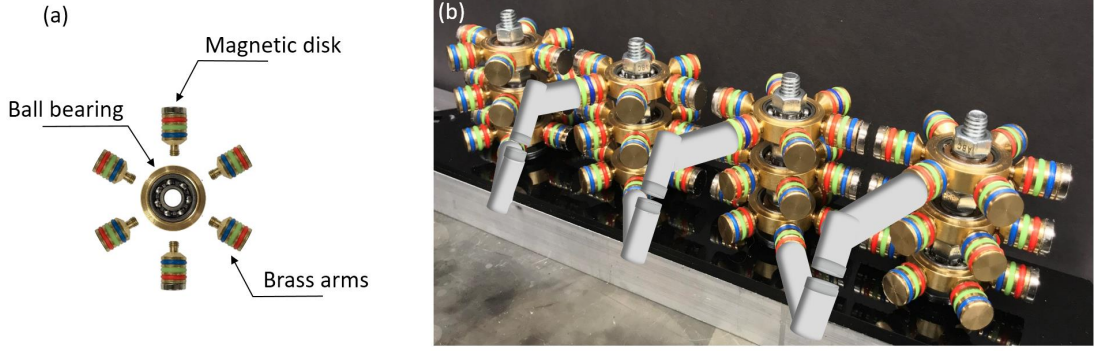


FIG. 1. **Magnetically coupled spinners: A versatile experimental platform.** (a) Example of the basic spinner configuration used in the present work. The arms are detachable such that the spinners can be easily refitted. (b) Exemplification of a relative complex linear configuration of coupled spinners.

the spinners will be pinned down, hence the spinner has only one degree of freedom, its orientation φ . By stacking and coupling such spinners, we can build extremely complex systems, one degree of freedom at a time. One such system is illustrated in Fig. 1(b). With such full control over the degrees of freedom and couplings, we can implement any quadratic Hamiltonian to drive the small oscillations of the coupled spinners.

The present work will feature a spinner with six grooved indentations and with heavy brass arms securely fastened in the brass encapsulation. Two of the arms are fitted with strong magnetic disks, which will provide the couplings between such identical spinners when the latter are arranged in linear patterns. These magnetic couplings can be measured by mapping the resonant modes of a dimer, whose dynamics is governed by the Lagrangian (I = moment of inertia):

$$L(\varphi_1, \varphi_2, \dot{\varphi}_1, \dot{\varphi}_2) = \frac{1}{2}I\dot{\varphi}_1^2 + \frac{1}{2}I\dot{\varphi}_2^2 - V(\varphi_1, \varphi_2). \quad (1)$$

In the regime of small oscillations around the equilibrium configuration $\varphi_1 = \varphi_2 = 0$, the potential can be approximated quadratically:

$$V(\varphi_1, \varphi_2) = \frac{1}{2}\alpha(\varphi_1^2 + \varphi_2^2) + \beta\varphi_1\varphi_2, \quad (2)$$

and the pair of the two resonant modes can be computed explicitly:

$$f_{\pm} = \sqrt{\frac{\alpha \pm \beta}{4\pi^2 I}}. \quad (3)$$

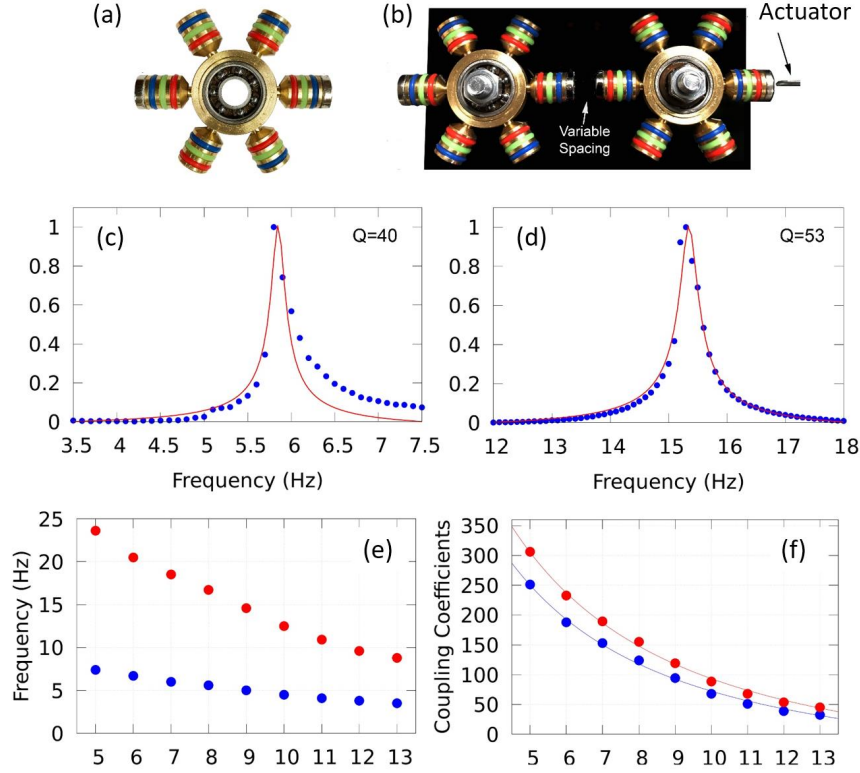


FIG. 2. **Mapping the coupling coefficients.** a) Illustration of a single spinner with the locations of magnets indicated. b) Experimental apparatus for measuring the interaction potential of a dimer. Two spinners are placed on an aluminum track with variable distance, d . The system is actuated and response is recorded using accelerometers. c) Experimentally measured low resonance of a dimer spaced 9 mm apart. The data indicate a quality factor of $Q = 40$. d) Experimentally measured high resonance of a dimer spaced 9 mm apart. The quality factor in this case is $Q = 53$. e) Map of the high (red) and low (blue) resonant modes as functions of magnet spacing. f) The coupling functions α and β as derived from (4).

The measured resonant frequencies are reported in Fig. 2 as functions of distance d between the magnets. Eqs. 3 can be inverted:

$$\alpha = 2\pi^2 I (f_+^2 + f_-^2), \quad \beta = 2\pi^2 I (f_+^2 - f_-^2), \quad (4)$$

which, together with the experimental data, enable us to determine the functional dependences $\alpha(d)$ and $\beta(d)$ of the coupling coefficients. The details are provided in Fig. 2 and note that units of $2\pi^2 I$ will be used from now on for the coupling functions.

When the centers of the spinners are pinned in a 1-dimensional pattern $\omega = \{x_n\}_{n \in \mathbb{Z}}$,

the Lagrangian of the system becomes:

$$L = \sum_{n \in \mathbb{Z}} \left[\frac{1}{2} I \dot{\varphi}_n^2 - \left(\alpha(d_n - 1) + \alpha(d_n) \right) \varphi_n^2 - \beta(d_n) \varphi_n \varphi_{n+1} \right], \quad d_n = x_{n+1} - x_n - D, \quad (5)$$

where D is the diameter of a spinner. The equation of motions read:

$$-I \ddot{\varphi}_n = \left(\alpha(d_{n-1}) + \alpha(d_n) \right) \varphi_n + \beta(d_{n-1}) \varphi_{n-1} + \beta(d_n) \varphi_{n+1}, \quad n \in \mathbb{Z}. \quad (6)$$

We encode the degrees of freedom in the column vector:

$$|\varphi\rangle = (\dots, \varphi_{-1}, \varphi_0, \varphi_1, \dots)^T, \quad (7)$$

and denote by $|n\rangle$ the column vector with 1 at position n and zero in rest. Then: $|\varphi\rangle = \sum_n \varphi_n |n\rangle$ and, with the ansatz $|\varphi(t)\rangle = \text{Re}\left[e^{i2\pi f t} |\psi\rangle\right]$ and the units from Fig. 2, the system of equations of motion becomes:

$$f^2 |\psi\rangle = H |\psi\rangle, \quad H = \sum_{n \in \mathbb{Z}} \left[\left(\alpha(d_{n-1}) + \alpha(d_n) \right) |n\rangle \langle n| + \beta(d_{n-1}) |n\rangle \langle n-1| + \beta(d_n) |n\rangle \langle n+1| \right]. \quad (8)$$

It is now a classical eigen-system for Hamiltonian H on the Hilbert space $\ell^2(\mathbb{Z})$.

We have presented the above analysis in detail because it can serve as a model for generically patterned resonators. For example, it can be straightforwardly implemented for other spinner configurations, even for the complex ones that include stackings and couplings beyond nearest-neighbors. During our exposition, especially when we discuss continuous deformations of the physical systems, it is extremely helpful to have a real physical realization in mind.

B. Aperiodic yet fully classifiable

To resolve the bulk-boundary correspondence principle for these systems, we inherently have to deal with the classification of gapped bulk Hamiltonians over the pattern ω . To properly define the latter, let us recall that our spinners can be easily reconfigured, hence the Hamiltonian (8) is only one of many Hamiltonians that we can implement over the pattern ω . Indeed, when we have N spinners stacked at each point of the pattern, then the Hilbert space becomes $\mathbb{C}^N \otimes \ell^2(\mathbb{Z})$, with elementary vectors of the form $\xi \otimes |n\rangle$,

and the most general Hamiltonian driving the small oscillations of the coupled spinners takes the form:

$$H_\omega = \sum_{n,n'} w_{n,n'}(\omega) \otimes |n\rangle\langle n'|, \quad w_{n,n'} \in M_N(\mathbb{C}), \quad w_{n',n} = w_{n,n'}^\dagger. \quad (9)$$

Throughout, $M_N(\mathbb{C})$ denotes the space of $N \times N$ matrices with complex entries. The above expression allows couplings beyond the first nearest neighbors and also allows for the coupling $N \times N$ matrices to depend on arbitrarily many geometrical data from the pattern ω . The coupling coefficients can be changed continuously, for example by modifying the strength of the magnets. Furthermore, by stacking a large number of spinners on top of each other at each point of the pattern, we can smoothly activate or de-activate internal degrees of freedom, hence change the dimension N . For the start, these will be the allowed continuous deformations of our physical systems. It is useful to view a gapped Hamiltonian as a pair (H_ω, G) , where G is a connected component of the resolvent set $\mathbb{R} \setminus \text{Spec}(H_\omega)$. Two gapped Hamiltonians (H_ω, G) and (H'_ω, G') are said to be in the same topological class if we can find a continuous gapped deformation connecting the two Hamiltonians. The topological classification of the gapped Hamiltonians consists of enumerating these topological classes as well as spelling out at least one representative for each class.

Since we are talking about generic aperiodic patterns, the topological classification may appear as a daunting task. To understand why this task is achievable, several key observations are in place:

1. The pattern ω needs to be treated as an ordinary variable. It takes values in the space of point patterns, a space that can be characterized and topologized using procedures that by now are quite standard[54]. Existence of a topology is important because we can then define what a continuous deformation of a point pattern is.
2. Recall that all spinners are identical copies of a basic design. Once the internal structure of the basic spinner is set, the functional dependences of the couplings on ω are fixed. More precisely, if we change the pattern to ω' , we will use the same functions $w_{n,n'}$ but evaluate them at ω' .
3. Per previous observation, a better terminology for the coupling coefficients would be coupling functions. This is in fact quite a useful concept, because ω , as a point in

the space of patterns, contains all the geometric information of the pattern and, in general, the coupling coefficients depend on many geometric details of the pattern. If the concept of coupling functions is adopted, then those complicated dependencies can be written concisely as $w_{n,n'}(\omega)$.

4. The coupling functions are assumed to be continuous of ω . We will also consider only cases where $w_{n,n'}(\omega)$ become negligible for n and n' far apart. Both assumptions are usually met in practice.

The particular Hamiltonian (8) definitely reflects all these principles, through the fact that $\alpha(d)$ and $\beta(d)$ have been measured once and then properly evaluated and applied to the arbitrary pattern ω . The analysis and the measurements that led to (8) can be repeated for more complex spinner structures and couplings, and the principles will surely emerge again. While they seem obvious, when taking full advantage of them, these observations bring a unique perspective, which is key to solving the topological classification.

Gearing towards that solution, note the natural action of the \mathbb{Z} group on the space of one-dimensional patterns:

$$\mathbb{Z} \ni a \rightarrow \tau_a \omega = \tau_a \{x_n\}_{n \in \mathbb{Z}} = \{x_{n+a} - x_a\}_{n \in \mathbb{Z}}. \quad (10)$$

We will always fix the point labeled by 0 at the origin of the real axis and set the labels to be consistent with the ordering $\dots < x_{-1} < x_0 = 0 < x_1 < \dots$. By this, we implicitly assume that two points are never on top of each other. Then τ_a can be identified with the rigid translation of the pattern that brings point x_a at the origin. Now, consistency requires that:

$$w_{n-a,n'-a}(\tau_a \omega) = w_{n,n'}(\omega) \Rightarrow w_{n,n'}(\omega) = w_{0,n'-n}(\tau_n \omega). \quad (11)$$

Dropping one redundant index and using $q = n' - n$, as well as the shift operator:

$$S|n\rangle = |n-1\rangle, \quad S^\dagger|n\rangle = |n+1\rangle, \quad SS^\dagger = S^\dagger S = I, \quad (12)$$

the generic Hamiltonian takes the form:

$$H_\omega = \sum_q \sum_n w_q(\tau_n \omega) \otimes |n\rangle\langle n| S^q, \quad (13)$$

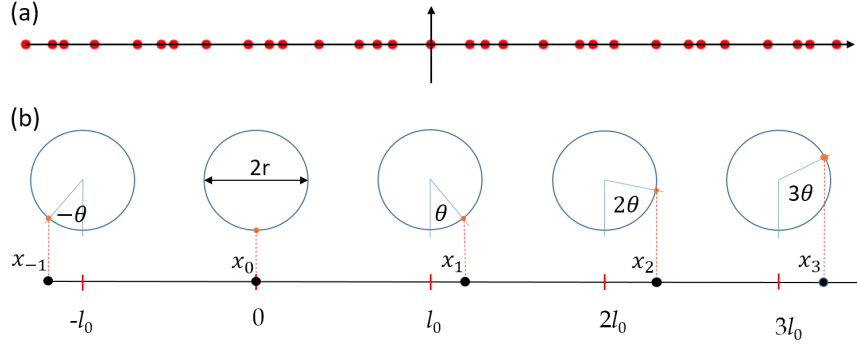


FIG. 3. **Example of a pattern with discrete hull equivalent to \mathbb{S}^1 .** a) Display of a finite number of points of a pattern generated by the algorithm $x_n = n l_0 + r \sin(n\theta)$, with the particular values $l_0 = 1, r = 0.4$ and $\theta = \frac{2\pi}{\sqrt{15}}$. b) A geometric algorithm to generate the same pattern, revealing that $\Xi \simeq \mathbb{S}^1$.

This expression already reveals a very particular structure. Note also that, in order to reproduce H_ω , we only need to evaluate the coupling functions on a small subset of the space of patterns, namely:

$$\Xi = \overline{\{\tau_n \omega, n \in \mathbb{Z}\}}, \quad (14)$$

where the over-line indicates the topological closure of the otherwise discrete set of translated patterns. In the professional literature [54], the tuple (Ξ, τ) , which is a bona-fide topological dynamical system, is called the discrete hull of the pattern. A system is called homogeneous if the orbit $\{\tau_n \omega'\}_{n \in \mathbb{Z}}$ is dense in Ξ for any pattern $\omega' \in \Xi$. We will be dealing exclusively with homogeneous patterns.

The main conclusion of all these is that every single Hamiltonian over the pattern ω can be generated using just the shift operator S and diagonal operators of the form $\sum_n f(\tau_n \omega) |n\rangle \langle n|$ with f a continuous function over Ξ . As we shall see, in many instances, the algebra generated by these operators is very simple and connects to other well known and well studied algebras. Ultimately, completing the topological classification program over a point pattern is conditioned by our ability to resolve the topological set Ξ and the action of \mathbb{Z} on it.

C. Generating patterns with prescribed hull

We will generate here a class of patterns for which Ξ is topologically equivalent with the circle \mathbb{S}^1 . The simplest pattern is illustrated in Fig. 3(a) and it has the analytic expression:

$$x_n = n l_0 + r \sin(n\theta), \quad r < \frac{l_0}{2}, \quad n \in \mathbb{Z}. \quad (15)$$

We will use the geometric algorithm explained in Fig. 3(b) to formally derive that $\Xi \simeq \mathbb{S}^1$. For this, consider a rigid translation $\tau_a \omega$ of the pattern, such that the old x_a now sits at the origin of the real axis. Associated this x_a there is a point on the circle and it is evident that knowing where this point is located enables us to reproduce the entire translated pattern $\tau_a \omega$. Indeed, we just need to apply the geometric algorithm described in Fig. 3(b) but this time starting from angle $a\theta$ instead of 0. This establishes a one to one relation between the translated patterns $\tau_a \omega$ and the angles $a\theta$, $a \in \mathbb{Z}$. For θ irrational (in units of 2π), these points densely fill the circle. We should note that Ξ is just a topological space and it has not geometry. From topological point of view, any closed loop is also a circle, hence more complex patterns can be generated by the same algorithm but using a deformed circle. Such pattern is illustrated in Fig. 4(a) and, as one can see, although the algorithm is simple, the resulting patterns can be extremely complex and irregularly looking. Using the same arguments, one can quickly see that Ξ is just the closed loop traced in Fig. 4(b), hence $\Xi \simeq \mathbb{S}^1$.

Based on the above remarks, one can see that we can actually allow not only continuous deformations of the resonators but also of the patterns themselves, provided the topology of the hull remains unchanged. This will be assumed from now on and will be covered by our topological classification.

III. THE C^* -ALGEBRAIC APPROACH

Here we formalize the algebra discovered in the previous chapter. It is instructive to inspect the commutation relations between the basic operators, which for $N = 1$ are:

$$\left(\sum_n f(\tau_n \omega) |n\rangle \langle n| \right) S = S \left(\sum_n f(\tau_n \omega) |n-1\rangle \langle n-1| \right) = S \left(\sum_n f(\tau_{n+1} \omega) |n\rangle \langle n| \right). \quad (16)$$

We see from here that, when conjugating the specific diagonal operators by S , f was effectively replaced by $f \circ \tau_1$. This observation will enable us to define an abstract algebra

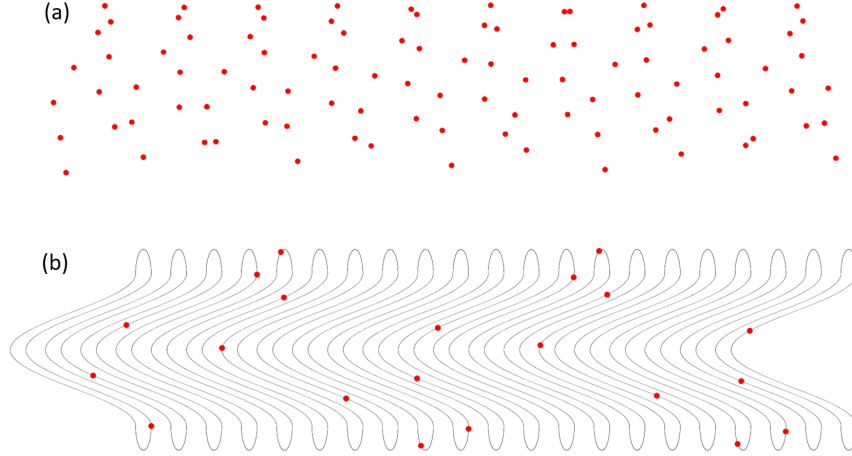


FIG. 4. **Additional example of a pattern with discrete hull equivalent to \mathbb{S}^1 .** a) Display of a finite number of points. b) The geometric algorithm used to generate the pattern consists of translation by θ along the loop followed by a horizontal translation by one unit.

which generates all Hamiltonians H_ω for all $\omega \in \Xi$.

A. The algebra of bulk physical observables.

We will discuss three important aspects even though some might appear technical at first sight. First, the definition of the algebra \mathcal{A} of bulk physical observables. It is the universal C^* -algebra generated by the algebra $C_N(\Xi)$ of continuous function over Ξ with values in $M_N(\mathbb{C})$ and by a unitary operator u ($uu^* = u^*u = 1$), satisfying the commutation relations which stem directly from (16):

$$fu = u(f \circ \tau_1), \quad \forall f \in C_N(\Xi). \quad (17)$$

A generic element from this algebra takes the form $a = \sum_q a_q u^q$, where all coefficients a_q are from $C_N(\Xi)$. The canonical representation on $\mathbb{C}^N \otimes \ell^2(\mathbb{Z})$ is provided by:

$$C_N(\Xi) \ni f \rightarrow \pi_\omega(f) = \sum_n f(\tau_n \omega) \otimes |n\rangle\langle n| \quad \text{and} \quad u \rightarrow S, \quad (18)$$

which we already verified in (16) to respect the commutation relations of \mathcal{A} . One can see explicitly that $\pi_\omega(h)$, $h = \sum_q w_q u^q$, generates (13). The algebra \mathcal{A} generates not only the Hamiltonians but all covariant physical observables over the patterns from Ξ , that is, the

families of operators $\{A_\omega\}_{\omega \in \Xi}$ with the property:

$$S^{-n}A_\omega S^n = A_{\tau_n \omega}, \quad \forall \omega \in \Xi. \quad (19)$$

Secondly, since one of the main themes is the classification under continuous deformations, we need to introduce a norm for \mathcal{A} in order to make precise what the latter means. The canonical norm on \mathcal{A} is:

$$\|a\| = \sup_{\omega \in \Xi} \|\pi_\omega(a)\|, \quad (20)$$

where on the right is the ordinary operator norm. When completed under (20), \mathcal{A} becomes a separable C^* -algebra, which for our program is extremely important because these algebras have well defined topological K -theories and their K -groups are always countable. In other words, we are assured that we have a sensible and useful topological classification.

Thirdly, there is an important relation between the spectrum of an element $h \in \mathcal{A}$ and the spectra of operators $\pi_\omega(a)$ that stems from it. Let us recall that the resolvent set of a is:

$$\text{Res}(a) = \{\lambda \in \mathbb{C} \mid (\lambda - a)^{-1} \text{ exists as an element of } \mathcal{A}\}. \quad (21)$$

The spectrum of a is then $\text{Spec}(a) = \mathbb{C} \setminus \text{Res}(a)$, a definition that actually makes sense for an arbitrary algebra. In general, we have the isomorphism:

$$\mathcal{A} \simeq \bigoplus_{\omega \in \Xi} \pi_\omega(\mathcal{A}) \quad \Rightarrow \quad \text{Spec}(h) = \bigcup_{\omega \in \Xi} \text{Spec}(H_\omega). \quad (22)$$

However, for a homogeneous system, $\text{Spec}(H_\omega)$ is independent of ω and, as such:

$$\text{Spec}(h) = \text{Spec}(H_\omega) \quad \forall \omega \in \Xi, \quad (23)$$

a conclusion which will play an important role in our final discussion.

B. Explicit computations.

If the pattern ω is periodic, then Ξ is just a point and the algebra \mathcal{A} is generated just by the shift operator S , hence it is commutative and we are dealing with the ordinary band theory.

If ω is a disordered lattice, *i.e.* small random displacements drawn from the interval $[-r, r]$ of otherwise equally spaced points, then Ξ is the Hilbert cube $[-r, r]^{\mathbb{Z}}$. This space has trivial topology since it is contractible to a point and, as a result, the K -theory of the resulting observable algebra is the same as the K -theory of the periodic lattice [27].

The simplest example with a non-trivial topology is when Ξ is equivalent to the circle and τ_1 is the translation by a fixed θ , as in the examples from Figs. 3 and 4. For $N = 1$, we know from the ordinary Fourier analysis that the algebra $C(\Xi)$ is generated by one function, $v(s) = e^{is}$, where s is the coordinate along the Ξ , assumed to be a closed loop of length 2π . We can compute the commutation relations (17) explicitly:

$$v u = u (v \circ \tau_1) = e^{i\theta} u v, \quad [\text{because } (v \circ \tau_1)(s) = e^{i(s+\theta)} = e^{i\theta} v(s)]. \quad (24)$$

The conclusion is that \mathcal{A} is just the non-commutative 2-torus. This is the same algebra as the one generated by the magnetic translations, from where one draws the Hamiltonians for electrons hopping on a lattice in a perpendicular uniform magnetic field. The latter is the setting where the Integer Quantum Hall Effect (IQHE) is observed, the prototypical topological system from class A in 2-dimensions. As we shall see, there are extremely close spectral and topological similarities between the two cases.

The point of these exercises was to convey that if (Ξ, τ) can be resolved and is simple enough, then the algebra \mathcal{A} can be computed explicitly and, in many cases, it can be connected with already well studied algebras. In these cases, the classification of the gapped Hamiltonians can be fully carried out and the bulk-boundary principle can be formulated very precisely. The latter will be exemplified in the coming sections.

IV. DECIPHERING THE BULK

A. Facts and observations.

The resonant frequency spectrum for Hamiltonian (8) over the pattern (15) is shown in Fig. 5(a), as function of parameter θ . The calculation was performed on a finite pattern of length $L = 840$ with periodic boundary condition, for all commensurate values $\theta_n = \frac{2n\pi}{L}$ (note that the spectrum is known to be continuous of θ , hence the use of rational values is not an issue here). The empirical couplings α and β have been used in these calculations.

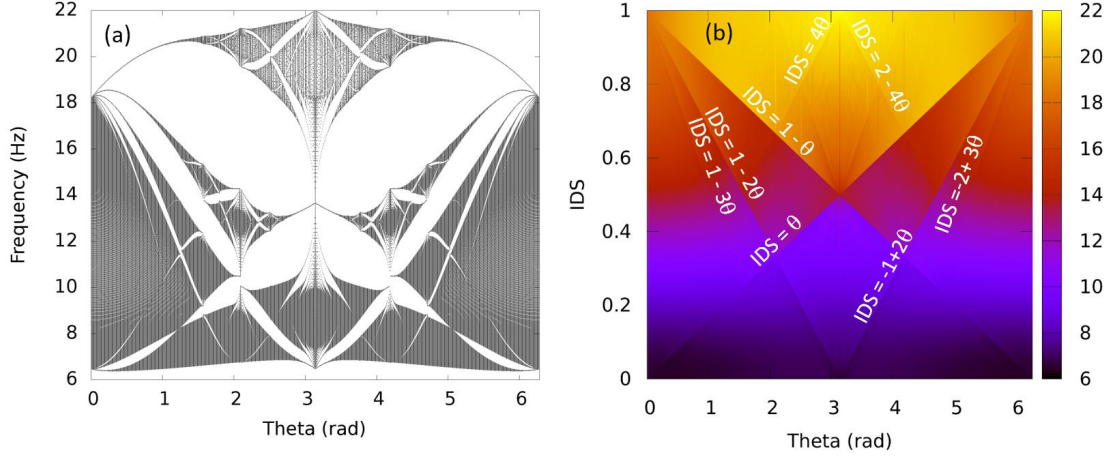


FIG. 5. **Bulk spectral characteristics of the Hamiltonian (8) over the pattern from Fig. 3.** (a) Bulk spectrum as function of parameter θ . The parameters l_0 and r have been fixed to the experimental values (see Fig. 6). (b) Integrated density of states (25) rendered as function of θ and frequency. The frequency axis is out of the plane.

As one can see, the similarity between this spectrum and the Hofstadter spectrum [28] is remarkable. The main characteristics of the spectrum is the fractal network of spectral gaps. Despite its complexity, the spectral gaps can be labeled uniquely by just two integer numbers [29]. A practical way to achieve this labeling is to compute the integrated density of states (IDS), defined as:

$$IDS(f) = \frac{\# \text{ resonant frequencies below } f}{\text{Length } L} \Bigg|_{L \rightarrow \infty}. \quad (25)$$

A graphic representation of IDS as function of f and parameter θ is reported in Fig. 5(b), as derived from the data reported in Fig. 5(a). In this rendering, the sharp changes in color are associated with the spectral gaps and, as one can see, the value of IDS inside the spectral gaps are all characterized by straight lines:

$$IDS(\theta) = n + m \theta, \quad n, m \in \mathbb{Z}. \quad (26)$$

Another key observation is that, since $N = 1$, IDS is always bound to the interval $[0, 1]$. As we shall see later, the index m in (26) is the topological number which dictates the presence or absence of edge modes. Examining (26), we see that there are only two instances where $m = 0$, namely, when the states are fully depopulated ($IDS = 0$) or fully populated ($IDS = 1$). We can now anticipate the main finding of our work, namely, that

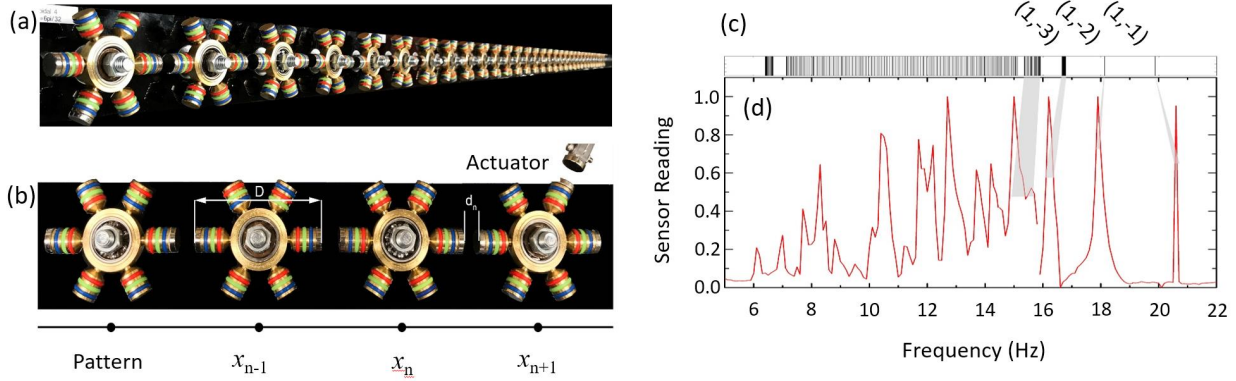


FIG. 6. **Experimental bulk spectral characteristics.** (a) A system of 32 spinners arranged in pattern (15). (b) Notations and experimental values: $\theta = \frac{6\pi}{32}$, $D = 66$ mm, $l_0 = 76$ mm, $r = 2$ mm. (c) Theoretically computed bulk spectrum for $\theta = \frac{2\pi}{\sqrt{117}} = \frac{6\pi}{32} + \mathcal{O}(10^{-3})$, together with the gap labels for the upper gaps, as extracted from Fig. 5. (d) Experimental reading from an accelerometer placed in the bulk of the system. The correspondence between theory and experiment is shown by the shaded regions.

every single gap seen in Fig. 5(a) is topological in the sense that $m \neq 0$ and, as we shall see, this automatically implies the emergence of topological edge states. This is a statement which applies to any Hamiltonian (13) with $N = 1$, hence it is an intrinsic characteristic of the pattern. By all measures, the pattern can be called topological.

For select values of θ , the bulk spectrum has been mapped experimentally. The setup is shown in Figs. 6(a,b). Throughout, our units for length will be millimeter. To accommodate for the diameter $D = 66$ mm of the spinners, their centers have been arranged according to the algorithm $x_n = 76n + 2 \sin(n\theta)$, $\theta = \frac{6\pi}{32}$, leading to a distance between the magnets (see Eq. 5):

$$d_n = 10 + 2 \sin((n+1)\theta) - 2 \sin(n\theta), \quad n \in \mathbb{Z}. \quad (27)$$

These are the inputs for Hamiltonian (8). The theoretically computed spectrum and the experimentally measured one are reported in Figs. 6(c,d), respectively. As one can see, the overall quantitative agreement is good, especially for the upper part of the spectrum. In fact, a rigorous correspondence between the two was established (see the guiding shaded regions in Figs. 6(c,d)), by matching the experimental and theoretical profiles of the normal modes.

Let us point out that the IDS is extremely difficult to map experimentally since the size of the system needs to be appreciable and each of the resonant frequencies need to be resolved. For these reasons, no attempt was made towards an experimental measurement.

B. Gap labeling: The K -theoretic account.

Perhaps one extremely puzzling question is how do the straight lines emerge in Fig. 5(b), given that no tuning of the coupling coefficients has been attempted. For example, identical straight lines will show up even if we arrange the spinners in the pattern shown in Fig. 4. The fundamental principle behind this phenomenon is easily explained by the K -theory of the observables algebra \mathcal{A} [29].

Some background, first. Given an element h of the C^* -algebra and a continuous function $\varphi : \mathbb{C} \rightarrow \mathbb{C}$, one can define a functional calculus $\varphi(h)$ by approximating φ by polynomials and taking the limit with respect to (20). This limit exists if and only if φ is continuous on the spectrum of h (see [55]). The example which will often appear from now on is the gap projection $p_G = \chi_{(-\infty, G]}(h)$, where h is the element of \mathcal{A} which generates a covariant family of gapped Hamiltonians (H_ω, G) . From now on, G will represent the gap itself and also an arbitrary point from the gap. Also, χ is the characteristic function of the specified interval. In the expression of p_G , $\chi_{(-\infty, G]}$ has a discontinuity at G but since it occurs outside the spectrum of h , p_G is indeed an element of \mathcal{A} , which generates the spectral projections of H_ω 's onto the spectrum below G . Consider now the family of functions $\varphi_t(x) = \frac{x-G}{1-t+t|x-G|}$, which interpolates continuously between $\varphi_0(x) = x$ and $\varphi_1(x) = \text{sgn}(x - G)$. Then, $\varphi_t(H_\omega)$ interpolates continuously between H_ω and $\text{sgn}(H_\omega) = 1 - 2\chi_{(-\infty, G]}(H_\omega)$. What this tells us is that classifying gap Hamiltonians (H_ω, G) is same as classifying the projections $P_\omega(G) = \chi_{(-\infty, G]}(H_\omega)$ or, at the level of algebra \mathcal{A} , the projections p_G . Typically, there are many projections in an algebra but, if they are organized in topological equivalence classes, their accountability becomes possible. This is what K -theory offers [25, 56–59].

Given a generic C^* -algebra \mathcal{A} , the K_0 group is defined as the classes $[p]_0$ of projections (*i.e.* $p^2 = p^* = p$) from $M_N(\mathbb{C}) \otimes \mathcal{A}$ with N arbitrarily large (hence $M_\infty(\mathbb{C})$ is used instead), where two projections belong to the same class iff they can be continuously deformed into each other or if there is $u \in M_\infty(\mathbb{C}) \otimes \mathcal{A}$ such that $p' = upu^*$ (when \mathcal{A} is tensored by $M_\infty(\mathbb{C})$, the two criterion coincide). Given two projections and their classes, one

defines $[p]_0 \oplus [q]_0 = \begin{pmatrix} p & 0 \\ 0 & q \end{pmatrix}_0$, which makes K_0 into an Abelian semi-group, which then can be completed to a group. This is how $K_0(\mathcal{A})$ group is defined. Similarly, two unitary elements from $M_\infty(\mathbb{C}) \otimes \mathcal{A}$ are declared from the same K_1 -class if they can be continuously deformed into each other. Given two unitaries and their K_1 -classes, one defines the binary operation $[u]_1 \odot [u']_1 = [uu']_1$, which transforms $K_1(\mathcal{A})$ into an Abelian group. Note that, since the projections and unitaries are drawn from $M_\infty(\mathbb{C}) \otimes \mathcal{A}$, we can simplify and take $N = 1$ in the definition of the bulk algebra, because $M_\infty(\mathbb{C})$ automatically takes care of the internal degrees of freedom!

The key observation is that, if \mathcal{A} is a separable C^* -algebra as in our case, then both $K_0(\mathcal{A})$ and $K_1(\mathcal{A})$ are at most countable. In fact, for the non-commutative 2-torus, which is the algebra associated to our patterns, $K_0(\mathcal{A}) \simeq \mathbb{Z}^2$ hence it has only two generators, the identity $[1]_0$ and the Rieffel projection $[p_\theta]_0$ [60]. As such, up to homotopies, any projection from $M_\infty(\mathbb{C}) \otimes \mathcal{A}$ can be decomposed as:

$$[p]_0 = [1]_0 \oplus \dots \oplus [1]_0 \oplus [p_\theta]_0 \oplus \dots \oplus [p_\theta]_0 = n [1]_0 + m [p_\theta]_0, \quad n, m \in \mathbb{Z}, \quad (28)$$

hence we can locate p in $K_0(\mathcal{A})$ using just the two integers n and m . As long as one classifies by K -theory, these integers represent the complete topological invariants that can be associated to a projection. It remains to show that they are the same numbers appearing in the IDS analysis. For this, note that the *IDS* values inside the gaps can be also computed as the trace per volume of the gap projections:

$$IDS(G) = \lim_{N \rightarrow \infty} \frac{1}{2N} \sum_{n=-N}^N \langle n | P_\omega(G) | n \rangle. \quad (29)$$

At the level of algebra \mathcal{A} , the trace per length has a very simple interpretation. Indeed:

$$\lim_{N \rightarrow \infty} \frac{1}{2N} \sum_{n=-N}^N \langle n | A_\omega | n \rangle = \lim_{N \rightarrow \infty} \frac{1}{2N} \sum_{n=-N}^N \langle n | \pi_\omega(a) | n \rangle = \lim_{N \rightarrow \infty} \frac{1}{2N} \sum_{n=-N}^N a_0(\tau_n \omega), \quad (30)$$

and, by using Birkhoff ergodic theorem [61], we can conclude that:

$$\lim_{N \rightarrow \infty} \frac{1}{2N} \sum_{n=-N}^N \langle n | A_\omega | n \rangle = \int_{\Xi} d\mathbb{P}(\omega) a_0(\omega), \quad (31)$$

where $\mathbb{P}(\omega)$ is the unique translation invariant probability measure on \mathbb{S}^1 . The right hand side defines a trace on the algebra \mathcal{A} which will be denoted by \mathcal{T} , *i.e.* a positive linear

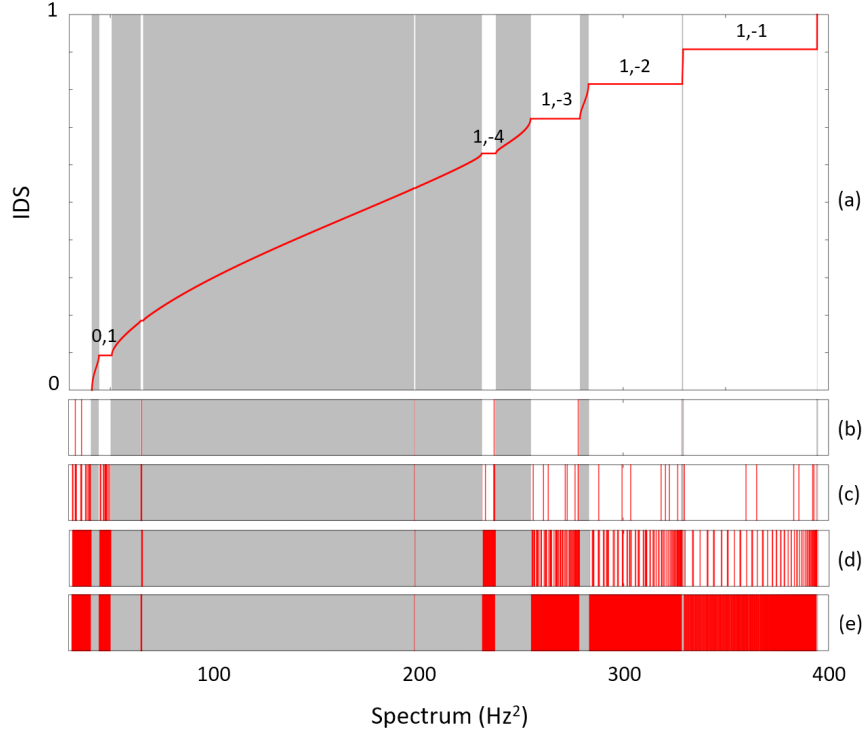


FIG. 7. **Numerical illustration of the topological edge spectrum.** (a) Integrated density of states (IDS) for the pattern (27) with $\theta = \frac{2\pi}{\sqrt{117}}$ (red curve). Overlaid in gray is the bulk spectrum. The IDS values $n + m\theta$ inside the spectral gaps are indicated by the pairs of integers (n, m) . (b-e) Edge spectrum (red marks) of N_s stacked edged systems, with $N_s = 1, 10, 100, 1000$, respectively. For convenience, the bulk spectrum is shown in gray.

functional such that $\mathcal{T}(aa') = \mathcal{T}(a'a)$ for any $a, a' \in \mathcal{A}$. Now, consider p and p' from the same K_0 -class. Then there exists u such that $p' = upu^*$ and consequently $\mathcal{T}(p) = \mathcal{T}(p')$. We have established that the trace is constant over the topological classes. In other words, it defines a topological invariant, in fact, the lowest one possible. Given the linearity [25, 29]:

$$IDS(G) = \mathcal{T}([p_G]_0) = \mathcal{T}(n[1]_0 \oplus m[p_\theta]_0) = n\mathcal{T}([1]_0) + m\mathcal{T}([p_\theta]_0) = n + m\theta, \quad (32)$$

where for the last equality we used the fundamental result $\mathcal{T}(p_\theta) = \theta$ [60].

Several observations are in place, with fundamental consequences for experiments. Given any Hilbert space \mathcal{H} , its algebra $\mathbb{B}(\mathcal{H})$ of bounded operators is not separable and its K -theory is irrelevant. In fact $K_0(\mathbb{B}) = 0$ for any separable \mathcal{H} [57]), so it is very important that the Hamiltonians over a pattern can be all drawn from the smaller algebra \mathcal{A} . The

number of internal degrees of the resonators cannot be fixed in general. In quantum chemistry, for example, we use pseudo-potentials and discard the deep electron states which are chemically inert and we also get rid of the states in the continuum spectrum. The tight-binding Hamiltonians used to model topological insulators are just effective Hamiltonians where an infinite number of internal states are “integrated out.” It is then important to acknowledge that, in K -theory, states can be added without changing the classification and this is why the K -theoretic classification is more physical than any other classification schemes (such as cohomology). Now an extremely fine and important point: note that, by definition, the labels n and m cannot be changed as long as p is continuously deformed. This deformation, however, needs to happen inside the algebra \mathcal{A} , by either deforming the resonators, the way they couple or by deforming the pattern without changing the topology of the discrete hull Ξ . These give the precise experimental conditions in which the predictions based on K -theory will hold, something which in the physical literature is completely overlooked yet it is paramount for the practical applications.

V. TOPOLOGICAL EDGE STATES

In this section we remove the degrees of freedom with index $n < 0$ and examine the spectral properties of the edged Hamiltonians, like:

$$\widehat{H}_\omega = \sum_{n,n' \geq 0} w_{n,n'}(\omega) \otimes |n\rangle\langle n'|, \quad w_{n,n'} \in M_N(\mathbb{C}), \quad w_{n',n} = w_{n,n'}^\dagger, \quad (33)$$

defined over the Hilbert space $\mathbb{C}^N \otimes \ell^2(\mathbb{N})$. The above Hamiltonians assumes that all spinners with $n < 0$ have been jammed. However, note that the edge can be generated in many different ways. For example, we could have removed all the spinners with index $n < 0$, in which case some of the coupling coefficients near the edge will be altered. In real-world applications, we will perhaps never be able to produce and maintain clean edges and, instead, the coupling constants will be drastically affected near the edge by the cutting process or by gradual wear and tear.

When a bulk system H_ω is edged to \widehat{H}_ω , the bulk spectrum remains in place but additional spectrum can emerged inside the bulk spectral gaps. It is useful to introduce

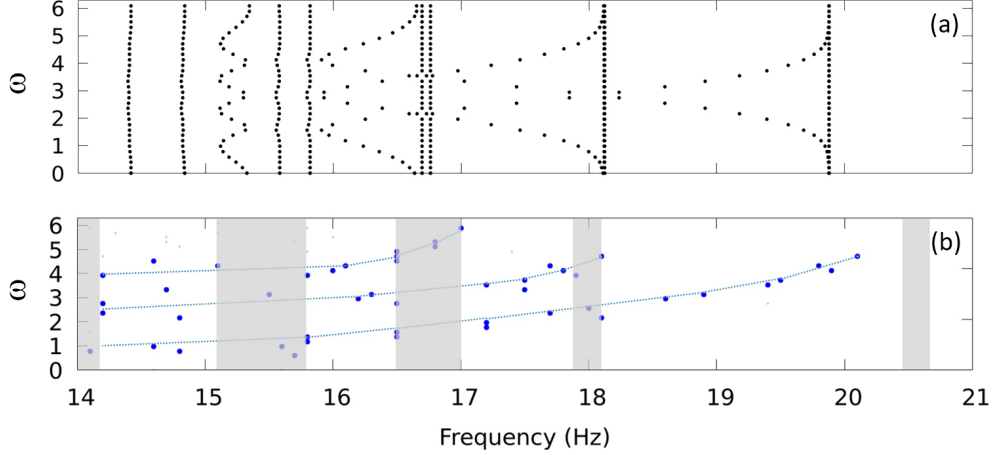


FIG. 8. **Theoretical edge spectrum versus the measured one.** The predicted theoretical edge spectrum is given on top as function of ω . As one can see, chiral bands appear crossing all bulk visible bulk gaps. Below, experimental data is shown with the bulk spectrum indicated by vertical grey bars. Red data indicates the right-most edge and blue the left-most. Dotted lines have been added to help indicate the chiral bands.

the edge spectrum as:

$$\text{Spec}_e(\widehat{H}_\omega) = \text{Spec}(\widehat{H}_\omega) \setminus \text{Spec}(H_\omega). \quad (34)$$

In one and quasi-one dimensional systems, $\text{Spec}_e(\widehat{H}_\omega)$ can only contain a finite number of eigenvalues. Interesting things can happen, however, when we stack the systems as $\widehat{H} = \bigoplus_{\omega \in \Omega} \widehat{H}_\omega$, in which case the bulk spectrum remains unchanged but the edge spectrum now consists of:

$$\text{Spec}_e(\widehat{H}) = \bigcup_{\omega \in \Xi} \text{Spec}_e(\widehat{H}_\omega) = \overline{\bigcup_{a \in \mathbb{Z}} \text{Spec}_e(\widehat{H}_{\tau_a \omega})}, \quad (35)$$

where in the last equality we used the fact that the orbit of ω is dense in Ξ . We call the edge spectrum topological if it fills the bulk gap completely and if it cannot be removed by any adiabatic deformation of the bulk system or by changing the boundary condition. Illustrating such topological spectrum and understanding the principle behind its existence and robustness are the main goals of this section.

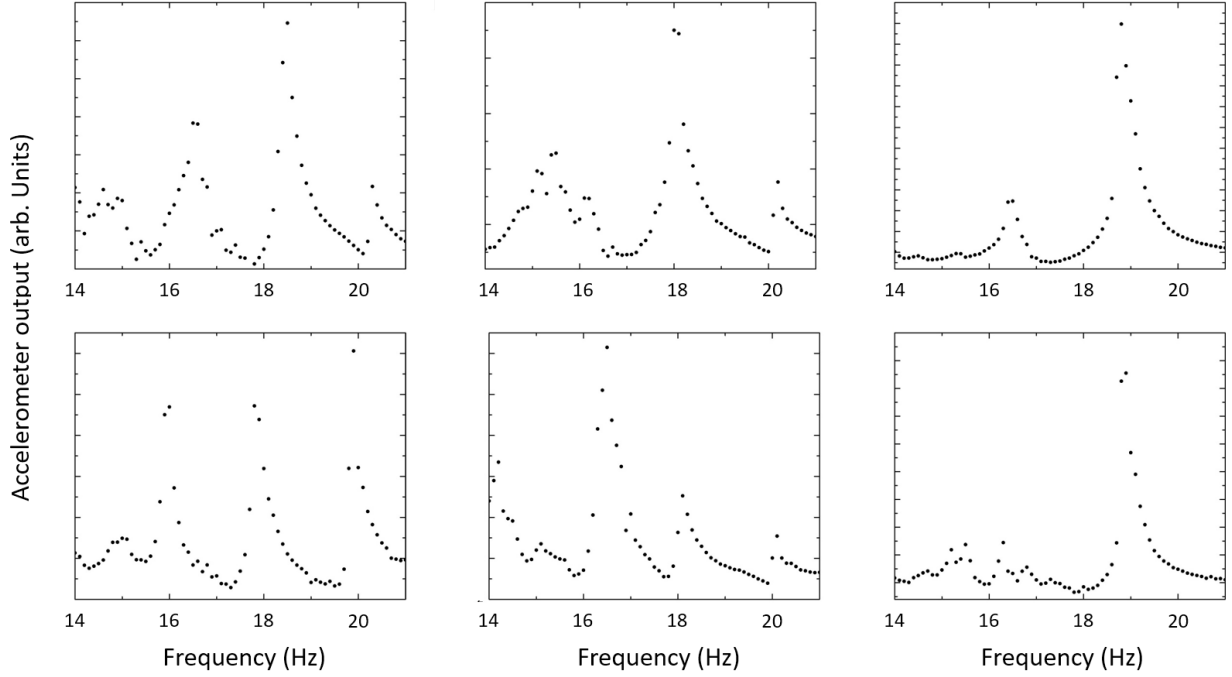


FIG. 9. **Measurements of the edge resonances.** The panels report the readings from accelerometers placed on the second spinner from the edge. They correspond to some arbitrarily selected rotated configurations of the spinner chain. The edge resonances appear as prominent peaks in these measurements.

A. Facts and observations

We present first numerical and experimental observations on the system of spinners with an edge. After removing all the spinners with index $n < 0$, the dynamics is described by the Hamiltonian:

$$\widehat{H}_\omega = \sum_{n \in \mathbb{N}} \left[\left(\alpha(d_{n-1}) + \alpha(d_n) \right) |n\rangle \langle n| + \beta(d_{n-1}) |n\rangle \langle n-1| + \beta(d_n) |n\rangle \langle n+1| \right], \quad (36)$$

with the understanding that $\alpha(d_{-1}) = \beta(d_{-1}) = 0$. In Fig. 7 we show the theoretically computed spectra of N_s stackings of edged systems:

$$\bigcup_{a=0, \dots, N_s-1} \text{Spec}(\widehat{H}_{\tau_a \omega}), \quad N_s = 1, 10, 100, 1000, \quad (37)$$

for the pattern (27) with the experimental coupling coefficients. The angle was fixed at $\theta = \frac{2\pi}{\sqrt{117}} \approx 0.5808$. We chose this particular irrational fraction of 2π because it accepts a good rational approximation $\theta = \frac{6\pi}{32} + \mathcal{O}(10^{-3})$, which will be conveniently used in

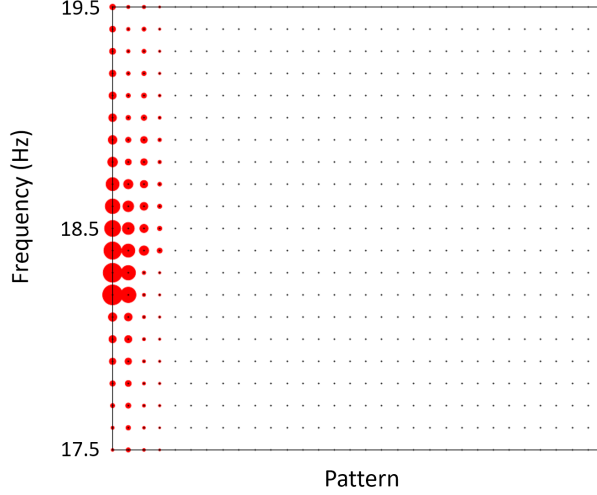


FIG. 10. **Spatial profile of a resonant mode.** The data reports the readings from four accelerometers placed on the first four spinners from the edge, as the frequency was swept over the last and most prominent bulk gap. The amplitudes of these readings are proportional with the size of the disks. For convenience, the full pattern of spinners is also shown.

the experiment. In the numerical calculations, however, the exact θ was used but the calculation was performed on a finite pattern with $L = 7669$, chosen based on the rational approximation $\theta = 2\pi\frac{709}{7669} + \mathcal{O}(10^{-7})$. This ensures that all graphical representations in Fig. 7 are extremely accurate.

Fig. 7(a) reports the computed *IDS* together with the gap labels (n, m) derived from the values of *IDS* inside the gaps. They are in agreement with the labels seen in Fig. 5. Examining Figs. 7(b-e), one can witness how all the spectral gaps of the bulk Hamiltonian are gradually filled with boundary spectrum as more systems are added to the stack. The resulting bundle of systems is topological in the sense described above, in full agreement with the gap labels. The edge spectrum can be resolved as function of $\omega \in \mathbb{S}^1$ as in Fig. 8, by noticing that the coordinate of $\tau_a\omega$ on the circle is the angle $a\theta$. The simulation in panel (a) shows that the edge spectrum splits in chiral bands, whose number equals the gap label m . Since the computation was performed on a finite rather than a halved system, the chiral bands appear always in pairs, one per edge.

The edge spectrum has been reproduced experimentally as reported in Fig. 8(b). In these experiments, the system shown in Fig. 6(a) has been actuate from the first or second

spinner from the edge, with a frequency that was varied in steps of 0.1 Hz from 14 to 21 Hz. One spinner was then moved from the front to back of the chain, effectively implementing the translation $\tau_1\omega$, and the measurements were repeated. By cycling this whole process, one can shift the pattern 32 times and generate the experimental measure of the edge spectrum (35). As the frequency is swept, topological edge modes are detected at proper frequencies inside the bulk spectral gaps. They manifest as extremely strong and well defined resonances, very clearly visible to the naked eye. A quantitative account of this phenomenon is reported in Fig. 9, which displays the reading from an accelerometer placed on the arm of the second spinner from the edge. Fig. 10 resolves the spatial profile of an edge resonant mode detected in the last and most prominent bulk gap. It confirms that the mode is extremely well localized near the edge.

B. The algebra of half-space observables

For the half-space, the shift operator, which on the new Hilbert space will be called \widehat{S} , is no longer unitary but instead:

$$\widehat{S}\widehat{S}^* = I, \quad \widehat{S}^*\widehat{S} = I - P_0, \quad P_0 = |0\rangle\langle 0|. \quad (38)$$

This suggests the definition of the half-space algebra $\widehat{\mathcal{A}}$ as the algebra generated by $C_N(\mathbb{E})$ and the operator \hat{u} satisfying the same commutation relations (17), but this time $\hat{u}^*\hat{u} = 1 - \hat{e}$, with \hat{e} a proper projection $\hat{e}^2 = \hat{e} \neq 1$. The half-space algebra accepts the following canonical representation:

$$C_N(\mathbb{E}) \ni f \rightarrow \hat{\pi}_\omega(f) = \sum_{n \geq 0} f(\tau_n\omega) \otimes |n\rangle\langle n| \quad \text{and} \quad \hat{\pi}_\omega(\hat{u}) = \widehat{S}, \quad (39)$$

which generates all half-space physical Hamiltonians [27]. In general $\widehat{\mathcal{A}} \simeq \bigoplus_{\omega \in \mathbb{E}} \hat{\pi}_\omega(\widehat{\mathcal{A}})$ hence:

$$\text{Spec}(\hat{h}) = \bigcup_{\omega \in \mathbb{E}} \text{Spec}(H_\omega) = \overline{\bigcup_{a \in \mathbb{Z}} \text{Spec}(H_{\tau_a\omega})} = \text{Spec}(\widehat{H}). \quad (40)$$

In other words, the spectrum of \hat{h} coincide with the spectrum of the stacked systems introduced and discussed above. This is important to keep in mind because the K -theoretic bulk-boundary principle contains a statement about the spectrum of \hat{h} , hence of the stacked systems, as already highlighted in Fig. 7.

Inside $\widehat{\mathcal{A}}$, there is the ideal $\widetilde{\mathcal{A}}$ made up of elements $\hat{a}\hat{b}$ for some $\hat{a}, \hat{b} \in \widehat{\mathcal{A}}$. When represented on the physical space, such elements are localized near the boundary, hence $\widetilde{\mathcal{A}}$ is called the boundary algebra [27]. Given a bulk Hamiltonian h , the half-space Hamiltonian with Dirichlet boundary condition, *i.e.* all couplings crossing the boundary set to zero, is generated by:

$$\hat{h}_D = \sum_{q \geq 0} h_q \hat{u}^q + \sum_{q < 0} h_q (\hat{u}^*)^{|q|}.$$

By adding elements from $\widetilde{\mathcal{A}}$, $\hat{h} = \hat{h}_D + \tilde{h}$, we can change the Dirichlet into any other boundary condition, hence the formalism is completely general. An important relation established in [27] is the isomorphisms between $\widetilde{\mathcal{A}}$ and $M_\infty(\mathbb{C}) \otimes C(\Xi)$, which will play an important role for the bulk-boundary correspondence principle. That is because then $K_*(\widetilde{\mathcal{A}}) = K_*(C(\Xi))$, and since $\Xi \simeq \mathbb{S}^1$, $K_*(\widetilde{\mathcal{A}}) \simeq \mathbb{Z}$. In particular, $K_1(\widetilde{\mathcal{A}})$ is generated by $[v]_1$, with v introduced in (24).

C. The engine of the bulk-boundary correspondence.

The following exact sequence between the algebras of physical observables is well established [26, 27]:

$$0 \longrightarrow \widetilde{\mathcal{A}} \xrightarrow{i} \widehat{\mathcal{A}} \xrightarrow{\text{ev}} \mathcal{A} \longrightarrow 0, \quad \text{ev}(\hat{u}) = u. \quad (41)$$

This exact sequence sets in motion a six-term exact sequence at the K -theory level [57–59]:

$$\begin{array}{ccccc} K_0(\widetilde{\mathcal{A}}) & \xrightarrow{i_*} & K_0(\widehat{\mathcal{A}}) & \xrightarrow{\text{ev}_*} & K_0(\mathcal{A}) \\ \text{Ind} \uparrow & & & & \downarrow \text{Exp} \\ K_1(\mathcal{A}) & \xleftarrow{\text{ev}_*} & K_1(\widehat{\mathcal{A}}) & \xleftarrow{i_*} & K_1(\widetilde{\mathcal{A}}) \end{array} \quad (42)$$

The relevance of this diagram to the bulk-boundary principle program was established by the work of Kellendonk, Richter and Schulz-Baldes [26]. Examining the right side of the diagram, one can see the standard K -theory map Exp taking projections from the bulk algebra into unitaries from the boundary algebras. It works as follows. Given a gapped bulk Hamiltonian (h, G) from \mathcal{A} , one defines a function $\phi : \mathbb{R} \rightarrow \mathbb{R}$ with a sharp but continuous variation in an ϵ -interval around any point G inside the gap, such that

$\phi = 0/1$ below/above that interval. Besides these requirements, ϕ is completely arbitrary. If \hat{h} is any half-space Hamiltonian obtained from h , *i.e.* $\text{ev}(\hat{h}) = h$, then [26, 27]:

$$\text{Exp}[p_G]_0 = [\tilde{u}_G]_1, \quad \tilde{u}_G = e^{2\pi i \phi(\hat{h})}. \quad (43)$$

As the notation suggests, \tilde{u}_G is a unitary element of the boundary algebra $\tilde{\mathcal{A}}$, because the function $e^{2\pi i \phi} - 1$ is non-zero only on the edge spectrum, hence $e^{2\pi i \hat{h}} - 1$ is built only from boundary states. If the half-space Hamiltonian \hat{h} is gapped, then we can take G and the variation of the function ϕ inside this gap, in which case ϕ is either 0 or 1 on the spectrum of \hat{h} . By the rules of functional calculus, \tilde{u}_G is just the identity. Phrase it differently, if \hat{h} is gapped, then $[p_G]_0$ is necessarily mapped into the trivial K_1 -class $[1]_1$ by the Exp map. On the other hand, if we know that the latter is not the case, then \hat{h} cannot be gapped. The key conclusion is that, if $\text{Exp}[p_G]_0 \neq [1]_1$ then topological boundary spectrum emerges, filling the **entire** bulk gap. This spectrum cannot be gapped by any boundary condition or adiabatic deformation of h .

To summarize, in order to establish a bulk-boundary correspondence principle, one needs to resolve the K -theories of both bulk and boundary algebras, as well as the action of Exp map on the generators of $K_0(\mathcal{A})$. We should warn the reader that just the condition $[p_G]_0 \neq [0]_0$ is in general not enough, a counter example being the case of Fibonacci patterns where the whole K_0 -group is mapped by the Exp map into the trivial K_1 -class of the boundary [45]. For our systems, these details are discussed next.

D. Topological patterns indeed.

From our analysis of the bulk, we know that $K_0(\mathcal{A})$ is generated by $[1]_0$ and $[e_\theta]_0$ and that every bulk gap projection accepts a decomposition:

$$[p_G]_0 = n[1]_0 + m[e_\theta]_0, \quad m \neq 0. \quad (44)$$

The action of the Exp map is also known [27] explicitly:

$$\text{Exp}[1]_0 = [1]_1, \quad \text{Exp}[e_\theta]_0 = [v]_1. \quad (45)$$

One can then see that any gap projection is mapped non-trivially:

$$\text{Exp}[p_G]_0 = m[v]_1 \neq [1]_1, \quad (46)$$

and, as a consequence, topological edge spectrum fills every single spectral gap of a bulk Hamiltonian, regardless of its particular form. Furthermore, (46) automatically implies that \tilde{u}_G is homotopic to v^m , hence m counts the winding of the eigenvalues of $\tilde{u}_G(\omega)$ as ω is varied along $\Xi \simeq \mathbb{S}^1$. In turns, this tells that m counts the number of chiral edge bands of \hat{h} , in agreement with the observations from Fig. 8.

In the cases when there are more internal degrees of freedom, $N > 1$, the *IDS* will take values in the interval $[0, N - 1]$, hence there are $N - 1$ possible instances where m in (32) can be zero. As such, among the infinite number of bulk gaps there will be only $N - 1$ gaps which are not topological, *i.e.* will not be filled with edge spectrum when the system is halved. If there is enough control over the design of a meta-materials, of course, one should try to isolate just one degree of freedom per resonator but, if this is not possible, even the cases with large N 's will still display plenty of topological gaps.

VI. DISCUSSION

We conclude with proposals of how our findings can be incorporated in practical applications. First, let us recall that the topological system singled out by our work consists of bundles or stacking of translates of H_ω . An important observation is that such bundles can be obtained by a simple and practical procedure. Indeed, by sequentially cutting equal pieces of length L from a single bulk sample and bundling them together, one is effectively generating $\bigoplus_{n \in \mathbb{N}} \widehat{H}_{\tau_{nL}\omega}$ (provided L is large enough). Since $\tau_{nL}\omega$ is densely sampling the configuration space Ξ , the desired stacking has been achieved.

The bundle described above will display edge modes which cannot be removed by cutting, tear and wear, or by gentle bending of the strands. Another important practical aspect is that the modes can be localized not only in space but also in frequency. Indeed, by examining the spectral butterfly in Fig. 5, one can see that, by varying θ , one can align at least one bulk spectral gap at any desired frequency within the bulk range.

Let us end by noting that our conclusions are not bound to mechanical systems and they apply to any coupled resonators regardless of their nature. Hence, whenever spatial and frequency control over the excitation modes is desired, the proposed patterns can

provide a convenient practical solution given the minimal tuning required.

- [1] E. Prodan, C. Prodan, *Topological phonon modes and their role in dynamic instability of microtubules*, Phys. Rev. Lett. **103**, 248101 (2009).
- [2] N. Berg, K. Joel, M. Koolyk, E. Prodan, *Topological phonon modes in filamentary structures*, Phys. Rev. E **83**, 021913 (2011).
- [3] L. Zhang, J. Ren, J.-S. Wang, B. Li, *The phonon hall effect: Theory and application*, J. Phys. Cond. Matt. **23**, 305402 (2011).
- [4] C. Kane, T. Lubensky, *Topological boundary modes in isostatic lattices*, Nature Physics **10**, 39-45 (2013).
- [5] B.-G. Chen, N. Upadhyaya, V. Vitelli, *Nonlinear conduction via solitons in a topological mechanical insulator*, Proc. Nat. Acad. Sci. **111**, 13004-13009 (2014).
- [6] A. B. Khanikaev, R. Fleury, S. H. Mousavi, A. Alu, *Topologically robust sound propagation in an angular-momentum-biased graphene-like resonator lattice*, Nature Comm. **6**, 8260 (2015).
- [7] P. Deymier, K. Runge, N. Swintek, K. Muralidharan, *Torsional topology and fermion-like behavior of elastic waves in phononic structures*, Comptes Rendus-Mecanique **343**, 700-711 (2015).
- [8] S. Mousavi, A. Khanikaev, Z. Wang, *Topologically protected elastic waves in phononic metamaterials*, Nature Comm. **6**, 8682 (2015).
- [9] V. Peano, C. Brendel, M. Schmidt, F. Marquardt, *Topological phases of sound and light*, Phys. Rev. X **5**, 031011 (2015).
- [10] J. Paulose, B.-G. Chen, V. Vitelli, *Topological modes bound to dislocations in mechanical metamaterials*, Nature Physics **11**, 153-156 (2015).
- [11] M. Xiao, W.-J. Chen, W.-Y. He, C. Chan, *Synthetic gauge flux and Weyl points in acoustic systems*, Nature Physics **11**, 920-924 (2015).
- [12] J. Paulose, A. Meeussen, V. Vitelli, *Selective buckling via states of self-stress in topological metamaterials*, Proc. Nat. Acad. Sci. **112**, 7639-7644 (2015).
- [13] Y.-T. Wang, P.-G. Luan, S. Zhang, *Coriolis force induced topological order for classical mechanical vibrations*, New Journal of Physics **17**, 073031 (2015).
- [14] M. Xiao, G. Ma, Z. Yang, P. Sheng, Z. Q. Zhang, C. T. Chan, *Geometric phase and band*

- inversion in periodic acoustic systems*, Nature Physics **11**, 240-244 (2015).
- [15] X. Mao, A. Souslov, C. Mendoza, T. Lubensky, *Mechanical instability at finite temperature*, Nature Comm. **6**, 5968 (2015).
- [16] T. Kariyado, Y. Hatsugai, *Manipulation of Dirac cones in mechanical graphene*, Scientific Reports **5**, 18107 (2015).
- [17] L. M. Nash, D. Kleckner, A. Read, V. Vitelli, A. M. Turner, W. T. M. Irvine, *Topological mechanics of gyroscopic metamaterials*, Proc. Nat. Acad. Sci. **112**, 14495-14500 (2015).
- [18] R. Süsstrunk, S. Huber, *Observation of phononic helical edge states in a mechanical topological insulator*, Science **349**, 47-50 (2015).
- [19] R. Süsstrunk, S. D. Huber, *Classification of topological phonons in linear mechanical metamaterials*, Proc. Nat. Acad. Sci. **113**, E4767-E4775 (2016).
- [20] P. Deymier, K. Runge, *One-dimensional mass-spring chains supporting elastic waves with non-conventional topology*, Crystals **6**, 44 (2016).
- [21] R. Pal, M. Schaeffer, M. Ruzzene, *Helical edge states and topological phase transitions in phononic systems using bi-layered lattices*, J. Appl. Phys. **119**, 084305 (2016).
- [22] G. Salerno, T. Ozawa, H. Price, I. Carusotto, *Floquet topological system based on frequency-modulated classical coupled harmonic oscillators*, Phys. Rev. B **93**, 085105 (2016).
- [23] D. Z. Rocklin, B. G. g Chen, M. Falk, V. Vitelli, T. C. Lubensky, *Mechanical Weyl Modes in Topological Maxwell Lattices*, Phys. Rev. Lett. **116**, 135503 (2016).
- [24] E. Prodan, K. Dobiszewski, A. Kanwal, J. Palmieri, Camelia Prodan, *Dynamical Majorana edge modes in a broad class of topological mechanical systems*, Nature Communications **8**, 14587 (2017).
- [25] J. Bellissard, *K-theory of C*-algebras in solid state physics*, in T. Dorlas, M. Hugenholtz, M. Winnink, editors, Lecture Notes in Physics **257**, 99-156, (Springer-Verlag, Berlin, 1986).
- [26] J. Kellendonk, T. Richter, H. Schulz-Baldes, *Edge current channels and Chern numbers in the integer quantum Hall effect*, Rev. Math. Phys. **14**, 87-119 (2002).
- [27] Prodan, E. & Schulz-Baldes, H. *Bulk and boundary invariants for complex topological insulators: From K-theory to physics*. (Springer, Berlin, 2016).
- [28] D. R. Hofstadter, *Energy levels and wave functions of Bloch electrons in rational and irrational magnetic fields*, Phys. Rev. B **14**, 2239-2249 (1976).
- [29] J. Bellissard, *Gap labeling theorems for Schroedinger operators*, in M. Waldschmidt, P.

- Moussa, J.-M. Luck, C. Itzykson eds., "From number theory to physics," (Springer, Berlin, 1995).
- [30] Y. E. Kraus, Y. Lahini, Z. Ringel, M. Verbin, O. Zilberberg, *Topological states and adiabatic pumping in quasicrystals*, Phys. Rev. Lett. **109**, 106402 (2012).
- [31] M. Verbin, O. Zilberberg, Y. E. Kraus, Y. Lahini, Y. Silberberg, *Observation of topological phase transitions in photonic quasicrystals*, Phys. Rev. Lett. **110**, 076403 (2013).
- [32] K. A. Madsen, E. J. Bergholtz, P. W. Brouwer, *Topological equivalence of crystal and quasicrystal band structures*, Phys. Rev. B **88**, 125118 (2013).
- [33] E. Prodan, *Virtual topological insulators with real quantized physics*, Phys. Rev. B **91**, 245104 (2015).
- [34] Y. E. Kraus, Z. Ringel, O. Zilberberg, *Four-dimensional quantum Hall effect in a two-dimensional quasicrystal*, Phys. Rev. Lett. **111**, 226401 (2013).
- [35] W. Hu, J. C. Pillay, K. Wu, M. Pasek, P. P. Shum, Y. D. Chong, *Measurement of a topological edge invariant in a microwave network*, Phys. Rev. X **5**, 011012 (2015).
- [36] Y. E. Kraus, O. Zilberberg, *Topological equivalence between the Fibonacci quasicrystal and the Harper model*, Phys. Rev. Lett. **109**, 116404 (2012).
- [37] D. Tanese, E. Gurevich, F. Baboux, T. Jacqmin, A. Lemaitre, E. Galopin, I. Sagnes, A. Amo, J. Bloch, E. Akkermans, *Fractal Energy Spectrum of a Polariton Gas in a Fibonacci Quasiperiodic Potential*, Phys. Rev. Lett. **112**, 146404 (2014).
- [38] D.-T. Tran, A. Dauphin, N. Goldman, P. Gaspard, *Topological Hofstadter insulators in a two-dimensional quasicrystal*, Phys. Rev. B **91**, 085125 (2015).
- [39] M. Verbin, O. Zilberberg, Y. Lahini, Y. E. Kraus, Y. Silberberg, *Topological pumping over a photonic Fibonacci quasicrystal*, Phys. Rev. B **91**, 064201 (2015).
- [40] E. Levy, A. Barak, A. Fisher, E. Akkermans, *Topological properties of Fibonacci quasicrystals : A scattering analysis of Chern numbers*, arXiv:1509.04028v3 (2015).
- [41] A. Dareau, E. Levy, M. B. Aguilera, R. Bouganne, E. Akkermans, F. Gerbier, J. Beugnon, *Direct measurement of Chern numbers in the diffraction pattern of a Fibonacci chain*, arXiv:1607.00901v1 (2016).
- [42] M. A. Bandres, M. C. Rechtsman, M. Segev, *Topological photonic quasicrystals: Fractal topological spectrum and protected transport*, Phys. Rev. X **6**, 011016 (2016).
- [43] F. Baboux, E. Levy, A. Lemaitre, C. Gómez, E. Galopin, L. L. Gratiet, I. Sagnes, A. Amo,

- J. Bloch, E. Akkermans, *Measuring topological invariants from generalized edge states in polaritonic quasicrystals*, Phys. Rev. B **95**, 161114(R) (2017).
- [44] A. Agarwala, V. B. Shenroy, *Topological Insulators in Amorphous Systems*, Phys. Rev. Lett. **118**, 236402 (2017).
- [45] J. Kellendonk, E. Prodan, *Bulk-Boundary Principle in Sturmian Kohmoto type models*, arXiv:1710.07681 (2017).
- [46] C. Bourne, E. Prodan, *Non-commutative Chern numbers for generic aperiodic discrete systems*, arXiv:1712.04136 (2017).
- [47] N. P. Mitchell, L. M. Nash, D. Hexner, A. Turner, W. T. M. Irvine, *Amorphous topological insulators constructed from random point sets.*, Nature Physics doi:10.1038 (2018).
- [48] M. Lohse, C. Schweizer, H. M. Price, O. Zilberberg, I. Bloch, *Exploring 4D Quantum Hall Physics with a 2D Topological Charge Pump*, Nature **553**, 55 (2018).
- [49] O. Zilberberg, S. Huang, J. Guglielmon, M. Wang, K. Chen, Y. E. Kraus, M. C. Rechtsman, *Photonic topological pumping through the edges of a dynamical four-dimensional quantum Hall system*, Nature **553**, 59 (2018).
- [50] D. Zhou, L. Zhang, X. Mao, *Topological edge floppy modes in disordered fiber networks*, Phys. Rev. Lett. **120**, 068003 (2018).
- [51] A. P. Schnyder, S. Ryu, A. Furusaki, A. W. W. Ludwig, *Classification of topological insulators and superconductors in three spatial dimensions*, Phys. Rev. B **78**, 195125 (2008).
- [52] S. Ryu, A. P. Schnyder, A. Furusaki, A. W. W. Ludwig, *Topological insulators and superconductors: tenfold way and dimensional hierarchy*, New J. Phys. **12**, 065010 (2010).
- [53] A. Kitaev, *Periodic table for topological insulators and superconductors*, (Advances in Theoretical Physics: Landau Memorial Conference) AIP Conference Proceedings **1134**, 22-30 (2009).
- [54] L. Sadun, *Topology of Tiling Spaces*, (American Mathematical Society, Providence, 2008).
- [55] W. Arveson, *A short course on spectral theory*, Graduate Texts in Mathematics, vol. 209, (Springer, Berlin, 2002).
- [56] K. R. Davidson, *C*-algebras by example*, (AMS, Providence, 1996).
- [57] N. E. Wegge-Olsen, *K-theory and C*-algebras*, (Oxford Univ. Press, Oxford, 1993).
- [58] B. Blackadar, *K-theory for operator algebras*, Volume 5 of Mathematical Sciences Research Institute Publications, (Cambridge Univ. Press, Cambridge, 1998).

- [59] M. Rordam, F. Larsen, N. Laustsen, *An Introduction to K-theory for C^* -algebras*, (Cambridge University Press, Cambridge, 2000).
- [60] M. A. Rieffel, *C^* -algebras associated with irrational rotations*, Pacific J. Math. **93**, 415-429 (1981).
- [61] G. D. Birkhoff, *Proof of the ergodic theorem*, Proc. Natl. Acad. Sci. USA **17**, 656-660 (1931).